Thallium isotopes reveal protracted anoxia during the Toarcian (Early Jurassic) associated with volcanism, carbon burial, and mass extinction

Theodore R. Them II[a,b,c,1], Benjamin C. Gill[c], Andrew H. Caruthers[d], Angela M. Gerhardt[c,e], Darren R. Gröcke[f], Timothy W. Lyons[g], Selva M. Marroquín[c], Sune G. Nielsen[h], João P. Trabucho Alexandre[i], and Jeremy D. Owens[a,b]

[a]Department of Earth, Ocean and Atmospheric Science, Florida State University, Tallahassee, FL 32306; [b]National High Magnetic Field Laboratory, Florida State University, Tallahassee, FL 32310; [c]Department of Geosciences, Virginia Polytechnic Institute and State University, Blacksburg, VA 24061; [d]Department of Geosciences, Western Michigan University, Kalamazoo, MI 49006; [e]Enervest Operating Company, Houston, TX 77002; [f]Department of Earth Sciences, Durham University, DH1 3LE Durham, United Kingdom; [g]Department of Earth Sciences, University of California, Riverside, CA 92521; [h]Department of Geology and Geophysics, Woods Hole Oceanographic Institution, Woods Hole, MA 02543; and [i]Department of Earth Sciences, Universiteit Utrecht, 3508 TC Utrecht, The Netherlands

Edited by Donald E. Canfield, Institute of Biology and Nordic Center for Earth Evolution, University of Southern Denmark, Odense M., Denmark, and approved May 16, 2018 (received for review February 28, 2018)

For this study, we generated thallium (Tl) isotope records from two anoxic basins to track the earliest changes in global bottom water oxygen contents over the Toarcian Oceanic Anoxic Event (T-OAE; ∼183 Ma) of the Early Jurassic. The T-OAE, like other Mesozoic OAEs, has been interpreted as an expansion of marine oxygen depletion based on indirect methods such as organic-rich facies, carbon isotope excursions, and biological turnover. Our Tl isotope data, however, reveal explicit evidence for earlier global marine deoxygenation of ocean water, some 600 ka before the classically defined T-OAE. This antecedent deoxygenation occurs at the Pliensbachian/Toarcian boundary and is coeval with the onset of initial large igneous province (LIP) volcanism and the initiation of a marine mass extinction. Thallium isotopes are also perturbed during the T-OAE interval, as defined by carbon isotopes, reflecting a second deoxygenation event that coincides with the acme of elevated marine mass extinctions and the main phase of LIP volcanism. This suggests that the duration of widespread anoxic bottom waters was at least 1 million years in duration and spanned early to middle Toarcian time. Thus, the Tl data reveal a more nuanced record of marine oxygen depletion and its links to biological change during a period of climatic warming in Earth's past and highlight the role of oxygen depletion on past biological evolution.

Toarcian Oceanic Anoxic Event | Early Jurassic | thallium isotopes | carbon isotope excursion | large igneous province

The amount of oxygen dissolved in the modern ocean is decreasing (1, 2), due, in part, to the increasing concentration of greenhouse gases in the atmosphere. Similar scenarios have likely occurred throughout geologic history. For example, during transient intervals in the Mesozoic—known as oceanic anoxic events (or OAEs)—substantial increases in atmospheric greenhouse gases were linked to the volcanic emissions of large igneous provinces (LIPs); these changes are hypothesized as the primary driver of OAEs (3–5). Understanding the mechanisms underlying intervals of marine deoxygenation in Earth history, such as OAEs, is essential because they are intimately linked with ecological shifts and, specifically, marine mass extinctions (6). Additionally, they provide us with an analog for possible future changes in the long-term oxygen inventory of the ocean of our planet (7, 8).

The concept of an OAE was proposed by ref. 9 to explain the multiple ocean basin occurrences of coeval organic matter-rich sediments, or black shales, deposited at a wide range of water depths on the middle Cretaceous ocean floor. OAEs were defined as brief (<1 Ma) episodes of expansion and intensification of the oxygen minimum layer in the ocean. This expanding layer encroached on the seafloor of seamounts, submarine plateaus, and continental margins and resulted in enhanced burial of organic matter in widespread black shales. The broad temporal association of these black shales with positive excursions in the marine carbon isotope record was subsequently documented (10). These excursions have been interpreted to reflect the elevated burial of ^{13}C-depleted organic carbon during the OAE (e.g., refs. 4, 5, and 10–14). The concept of an OAE was later applied to a positive excursion in the carbon isotope record of Tethyan Lower Jurassic limestones during what is now known as the Toarcian OAE (T-OAE) (13).

Subsequent studies of the T-OAE identified an abrupt, large-magnitude, negative carbon isotope excursion (CIE) at *ca.* 183.1 Ma that interrupts a broader positive CIE noted by ref. 13. Generally, this negative CIE appears to define the onset of major environmental disruption, the onset of organic-rich deposition, and the main pulse of mass extinction (5, 15–17) (Fig. 1). A carbon isotope compilation of published work has also shown that the broader early Toarcian positive CIE actually begins at the Pliensbachian/Toarcian boundary (Fig. 1 and *SI Appendix*, Fig. S3) (5, 18, 19). However, this broader positive CIE precedes the onset of organic-rich deposition that defines the start of the T-OAE at many locations (refs. 5, 14,

Significance

Declining oxygen contents in today's oceans highlight the need to better understand ancient, natural marine deoxygenation and associated extinctions. In the Early Jurassic, the Toarcian Oceanic Anoxic Event (T-OAE; ∼183 Ma) is associated with significant perturbations to the Earth system, historically defined by carbon isotopes. We reconstructed global oceanic (de)oxygenation using thallium isotopes from two ocean basins that suggest a stepwise decline of oxygen that initiated before and extended well after the classically defined T-OAE interval. This initial deoxygenation occurs with the start of massive volcanism and marine extinctions, while a later shift corresponds to the traditional T-OAE. This emphasizes the need for more nuanced records of ancient environmental and biogeochemical feedbacks that lead to and maintain widespread marine anoxia.

Author contributions: T.R.T., B.C.G., T.W.L., and J.D.O. designed research; T.R.T., B.C.G., A.H.C., A.M.G., S.M.M., and J.D.O. performed research; B.C.G., T.W.L., S.G.N., and J.D.O. contributed new reagents/analytic tools; T.R.T., B.C.G., A.H.C., D.R.G., T.W.L., S.G.N., J.P.T.A., and J.D.O. analyzed data; and T.R.T., B.C.G., A.H.C., S.G.N., and J.D.O. wrote the paper.

The authors declare no conflict of interest.

This article is a PNAS Direct Submission.

[1]To whom correspondence should be addressed. Email: themtr@cofc.edu.

This article contains supporting information online at www.pnas.org/lookup/suppl/doi:10.1073/pnas.1803478115/-/DCSupplemental.

Published online June 11, 2018.

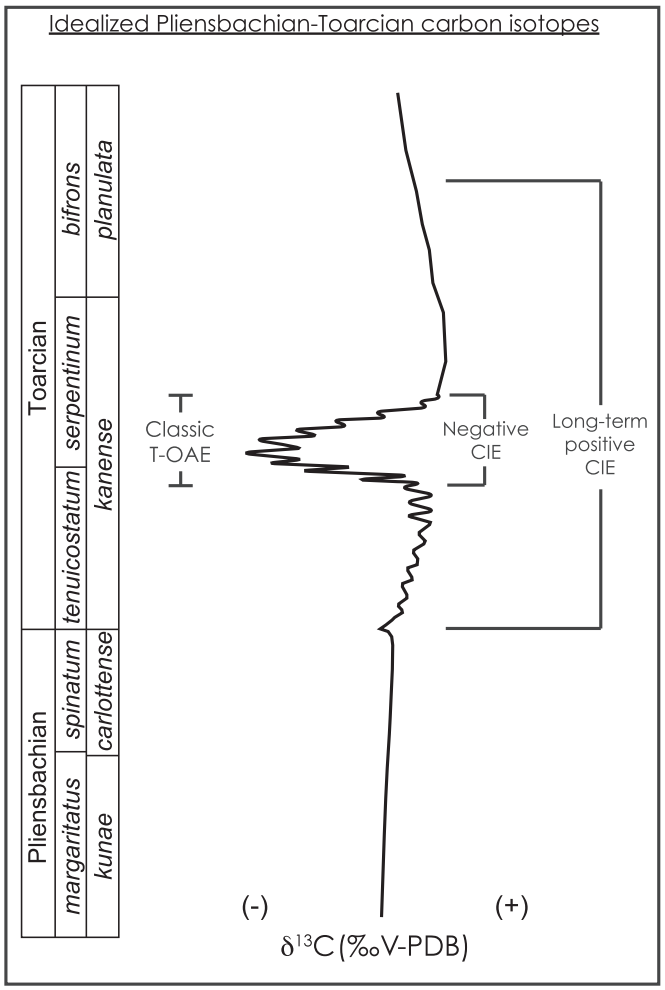

Fig. 1. Idealized Pliensbachian and Toarcian carbon isotope stratigraphy (derived from multiple $\delta^{13}C$ records from Europe, northern Africa, and North America shown in *SI Appendix*, Fig. S3). Note the long-term positive CIE predating the negative CIE associated with the classic T-OAE interval.

and many others) (Fig. 1 and *SI Appendix*, Fig. S3); thus it has not been generally considered part of the T-OAE. This interval is also intriguing because it corresponds to the beginning of a mass extinction that later reaches its climax during the T-OAE (17).

Although positive CIEs could represent the effects of large-scale oxygen depletion in seawater, other environmental variables can contribute to the carbon isotope record (20, 21), and there is no simple relationship between redox conditions and organic matter preservation (ref. 22, as reviewed by ref. 23). Thus, the culmination of a positive CIE does not require global ocean deoxygenation or even increased organic carbon burial (20, 22–25), as carbon isotopes ultimately track the balance of all of the input and output fluxes and associated isotope fractionations (20). For this reason, carbon isotope data cannot be used alone as a proxy for the expansion of oceanic anoxia. Additionally, evidence for decreasing marine oxygen inventories leading to OAEs is hampered, since redox proxies typically constrain the most extreme euxinic (oxygen-free, sulfide-containing waters) end member (26–29). As such, uniquely constraining the global extent of nonsulfidic, anoxic waters has not been possible. This bias highlights the need for a more sensitive proxy that constrains more subtle changes in oceanic oxygen levels during OAEs and other oceanographic events in Earth history.

Using Thallium Isotopes to Track Global Marine Oxygen Contents

Thallium isotopes in organic matter-rich mudstones provide a novel window to secular variations in the oceanic oxygen inventory over the expanded T-OAE interval from the latest Pliensbachian to middle Toarcian (see *SI Appendix* for Tl isotope nomenclature). The modern open ocean seawater Tl isotope composition (with a residence time of *ca.* 20 ka) is homogenous to within <0.5 ε-units (30–32), and this seawater value is captured in the sediments deposited in euxinic settings (32). Thallium is introduced to the ocean by rivers, high-temperature hydrothermal fluids, volcanic emissions, mineral aerosols, and pore-water fluxes from continental margin sediments. These sources have essentially identical Tl isotopic compositions of $\varepsilon^{205}Tl \approx -2$ (as reviewed in ref. 33), which reflects minimal isotope fractionation during continental weathering and high-temperature mobilization of Tl. The major outputs of Tl from the marine system include adsorption onto manganese (Mn) oxides and, low-temperature (<100 °C) alteration of oceanic crust (AOC). Sedimentation of organic matter and sulfide minerals in low oxygen settings also removes Tl from seawater, but the global flux is relatively minor in the modern ocean (32, 34). Adsorption onto Mn oxides and AOC are the only known processes that fractionate Tl.

Specifically, Mn oxides are heavier than seawater by ∼+13 ε-units to 19 ε-units, which is likely due to equilibrium isotope fractionation during oxidation of univalent aqueous Tl to trivalent Tl when permanently sorbed to Mn oxides (33, 35, 36). The uncertainty associated with the Tl isotope fractionation factor during sorption to Mn oxides relates to Tl isotope variations found in some pelagic clays with somewhat less positive compositions (37). However, pure Mn oxides as found in Fe–Mn crusts display relatively constant offsets from seawater of $\sim+19 \pm 2$ ε-units (30, 33), which is the preferred value for Tl isotope fractionation during sorption to Mn oxides.

The mechanism of Tl isotope fractionation during incorporation into AOC is less well understood but is likely a kinetic process whereby the light isotope is preferentially incorporated into AOC (33). Although individual samples of AOC can exhibit $\varepsilon^{205}Tl \approx -15$ (38), the average is more likely closer to $\varepsilon^{205}Tl \approx -7$, because uptake is close to quantitative from the circulating hydrothermal fluids (33); thus the fractionation from seawater is minimal.

Although the marine Tl residence time is long enough to produce a globally homogenous Tl isotope composition of the ocean, it is still short enough that seawater $\varepsilon^{205}Tl$ can respond to rapid global changes in Mn oxide burial on glacial–interglacial timescales (33, 39). In contrast, AOC depositional fluxes vary on extremely long timescales ($>10^7$ y) as these respond primarily to global average seafloor spreading rates (40), and, hence, $\varepsilon^{205}Tl_{seawater}$ variations on timescales shorter than ∼1 My are most likely driven by changes in Mn oxide preservation and burial. Crucially, Mn oxides are only buried in sediments with O_2 present at or near the sediment/water interface, because they are rapidly dissolved under anoxic conditions (41). In turn, global Mn oxide burial fluxes are related to the global extent of bottom water anoxia (32). As such, $\varepsilon^{205}Tl_{seawater}$ can be related to relative changes in oceanic oxygenation. Thallium isotopes have been applied to only one ancient climate perturbation that documents the global relationship between oceanic oxygenation leading up to the Cenomanian/Turonian event of OAE-2 (39), and it was shown that changes in carbon isotopes lagged the onset of marine deoxygenation, which underlines the potential for Tl isotopes to provide unique information about ancient oceanic oxygenation. During intervals of increased bottom water oxygen extent, $\varepsilon^{205}Tl_{seawater}$ values will be more negative, whereas during intervals of decreased bottom water oxygen extent (increase of bottom water anoxia), $\varepsilon^{205}Tl_{seawater}$ values will be more positive and approach their source value ($\varepsilon^{205}Tl = \sim-2$).

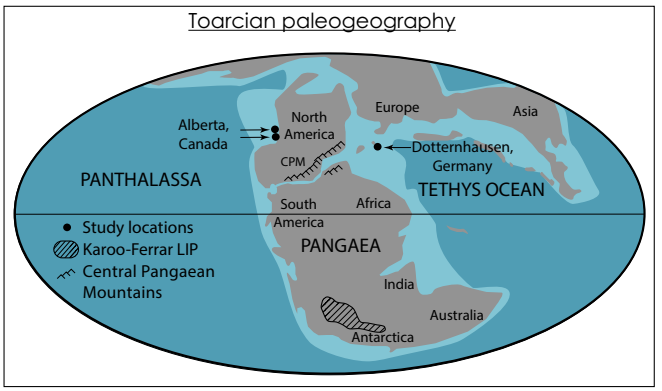

Fig. 2. Global paleogeography of early Toarcian. Black circles represent the study areas. Dashed extent of the Karoo–Ferrar LIP shown in southern Pangaea. Dark gray, landmasses; light blue, shallow seas; and dark blue, open oceans; CPM, Central Pangaean Mountains. Reprinted with permission from ref. 63.

Study Site Selection

To reconstruct global ocean oxygen contents (or redox changes) using the Tl isotope system, it is necessary to constrain local water column redox conditions to be sure to capture the seawater value, thus avoiding any local Mn oxide signatures. This is because variations in local sedimentary redox conditions and basinal restriction can influence the isotopic signals captured in the sedimentary record and can hamper the use of these records to reconstruct changes in global marine redox conditions (29, 34, 42, 43). Therefore, it is important to investigate multiple localities that were well connected to the open ocean and have independent constraints on local redox conditions (e.g., refs. 39 and 44). Here, we analyzed samples from two Lower Jurassic successions that contain intervals that were deposited under euxinic conditions—as identified by established, independent proxies for local redox, including Fe speciation—before, during, and after the T-OAE (Fig. 2 and *SI Appendix*, Figs. S1 and S2). We first investigated three Pliensbachian and Toarcian sections of the Fernie Formation from the Western Canada Sedimentary Basin, which represent deposition on an open-ocean margin of northeastern Panthalassa (Fig. 2). These samples were taken from outcrop (East Tributary) and two cores (1-35-62-20W5, 6-32-75-5W6). The other studied Toarcian succession, Dotternhausen Quarry, Germany, represents deposition in a semirestricted structural basin in the European epeiric sea, which was connected to the Tethys Ocean (45) (Fig. 2).

Results

Data from the base of the East Tributary section, within the Pliensbachian portion of the section (*Amaltheus margaritatus* Zone in northwest Europe and *Fanninoceras kunae* Zone in North America), start with an ε^{205}Tl of ~−6 (Fig. 3). These values are similar to the ε^{205}Tl of modern seawater (32) and suggest a similar global Tl isotopic mass balance tied to Mn oxide burial and similar extents of oxygenated bottom waters. At the Pliensbachian/Toarcian boundary, ε^{205}Tl gradually shifts to less negative values and remains steady until the onset of the negative Toarcian CIE. We interpret this initial rise in ε^{205}Tl as the beginning of the expansion of oceanic anoxia before the classically defined T-OAE (Fig. 1) with a date of ~183.65 Ma (±~0.150 Ma) (46), ~500 ky to 600 ky before the onset of the negative CIE (47, 48) that traditionally defines the base of the T-OAE. Furthermore, our δ^{13}C and ε^{205}Tl data from two drill cores from elsewhere in the Western Canada Sedimentary Basin show similar values and trends (*SI Appendix*, Figs S1 and S2), suggesting that they

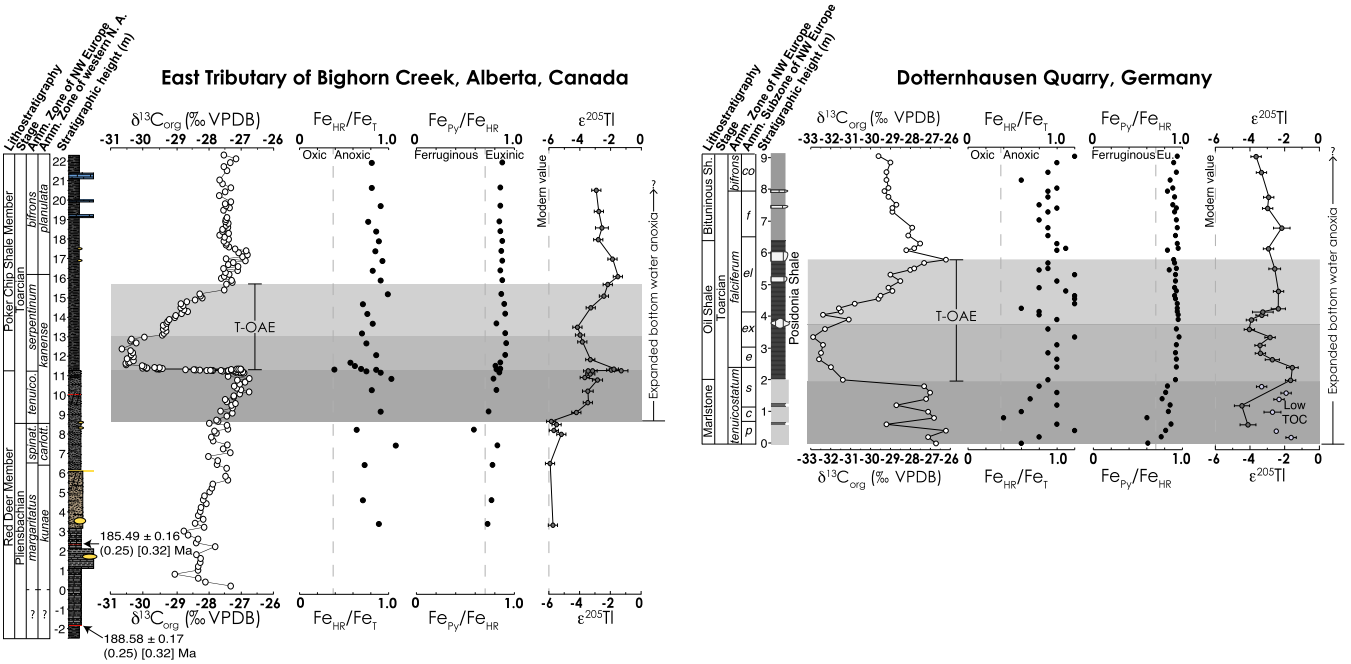

Fig. 3. Chemostratigraphy of the Lower Jurassic Fernie Formation from East Tributary of Bighorn Creek, Alberta and of the Lower Jurassic Posidonia Shale from the Dotternhausen Quarry in Germany; $\delta^{13}C_{org}$, organic carbon isotopic compositions from refs. 19 and 29; Fe_{HR}/Fe_T, amount of highly reactive iron relative to total iron; Fe_{Py}/Fe_{HR}, amount of pyrite iron relative to highly reactive iron (see *SI Appendix* for discussion of this redox proxy); ε^{205}Tl, thallium isotopic composition of seawater during deposition. Lithostratigraphic members of the Fernie Formation, stages of the Jurassic, and ammonite zonations for both northwestern Europe and western North America are shown to the left of the stratigraphic column (refer to ref. 19 and *SI Appendix* for the details of their placements). Vertical gray lines in ^{205}Tl records are the modern $^{205}Tl_{SW}$ composition of ~−6 (32). Light gray ε^{205}Tl values in the German section are from lithologies that are not ideal for many metal isotope studies (total organic carbon values are less than 0.3%), and we therefore do not interpret these as primary oceanographic signals (*SI Appendix*). Gray boxes represent CIE intervals. Data from refs. 19 and 29.

capture global signals and that Early Jurassic seawater ε^{205}Tl values were also homogenous.

The German Dotternhausen Quarry section (29, 45), where the Pliensbachian/Toarcian boundary is absent, shows time-equivalent ε^{205}Tl values (~−4) that are nearly identical, within analytical error, to results from Canada (~−3.5) for the lower Toarcian *Dactylioceras tenuicostatum* (equivalent) Zone (Fig. 3). The ε^{205}Tl values increase at the onset of the negative CIE, gradually decrease during the minimum of the CIE, and increase during the rising limb of the carbon isotope data (Fig. 3). A longer-term decrease of Tl isotopes occurs after the end of the negative CIE to the top of the section (Fig. 3). The similarities among all study sites support the interpretation that these Tl isotope records represent primary global ocean signals, even in the more restricted setting of the German section.

Discussion

The shift in Tl isotopes from −6 to −4, as observed at the Pliensbachian/Toarcian boundary (Fig. 3), based on isotope mass balance calculations, requires a ~50% decrease in the global burial of Mn oxides (32). In all likelihood, the decline in marine Mn oxide burial was linked to an expansion of bottom water anoxia, which restricted the area of oxic sediment deposition. This initial deoxygenation is notable because it generally coincides with (*i*) the interpreted onset of Karoo–Ferrar LIP activity (49, 50) at the start of the longer-term positive CIE, (*ii*) initiation of a radiogenic osmium isotope excursion (46, 51), and (*iii*) the beginning of a marine mass extinction event (beginning of phase 3 of ref. 17) (Fig. 4). These observations are consistent with marine deoxygenation caused by an increase in organic carbon export linked to enhanced chemical weathering and nutrient input to the oceans. This sequence led to increased oxygen consumption in the aphotic zone, driving the expansion of oxygen

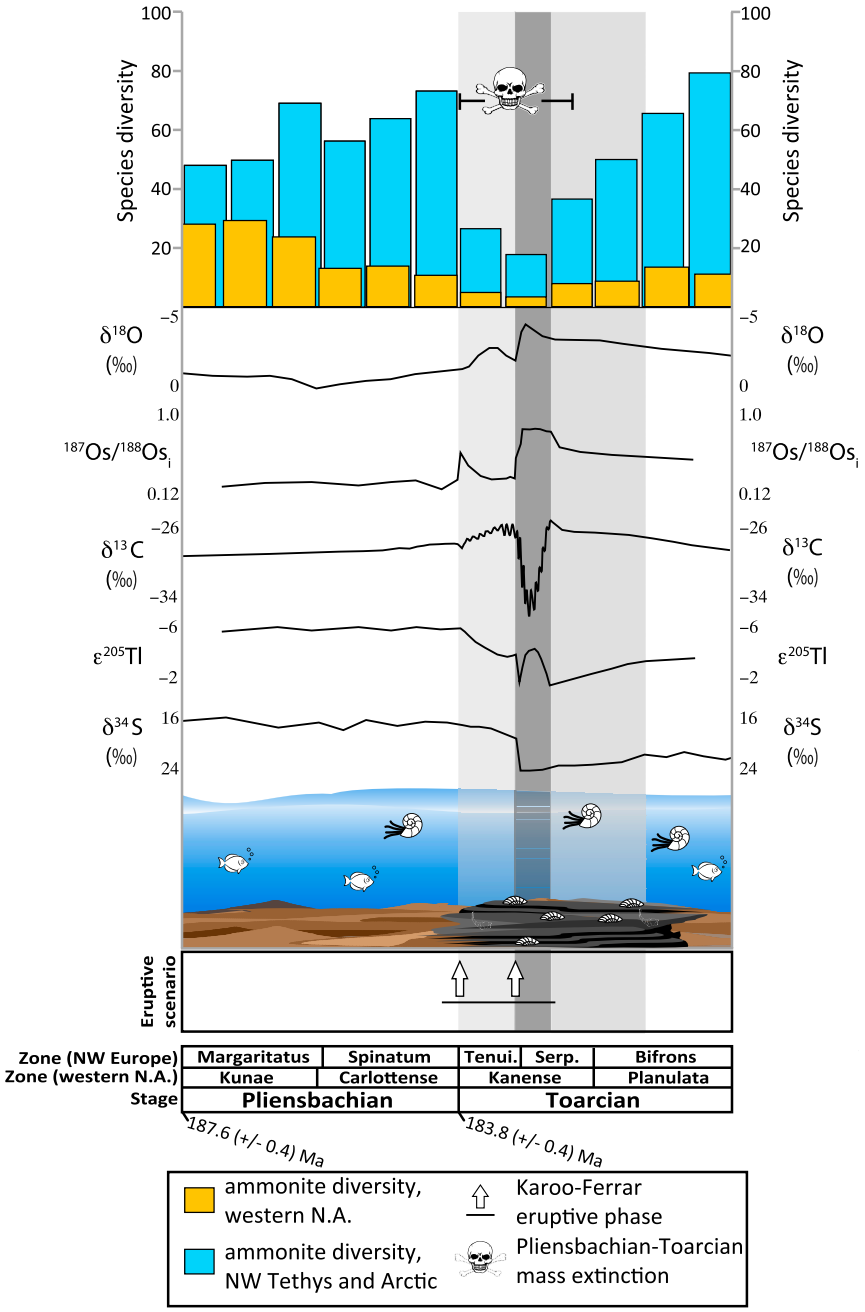

Fig. 4. Sequence of events culminating in the Early Jurassic T-OAE (as delineated by changes in the precipitation of manganese oxyhydroxides at the sediment–water interface, documented by shifts in the ε^{205}Tl composition of anoxic sediments) and carbon burial event (as delineated by changes to the global carbon cycle, documented by changes in the δ^{13}C of organic and inorganic carbon). As the Karoo–Ferrar LIP is emplaced (3, 49, 54), global ocean deoxygenation may occur concurrently as sea surface temperatures rise (64). Massive injections of greenhouse gases and cascading biogeochemical feedbacks cause the second decline in biodiversity associated with the T-OAE negative CIE interval. The extent of anoxic marine bottom waters increases as bioproductivity increases due to increased continental weathering and delivery of nutrients to the oceans (46, 51), leading to the increased geographic extent of euxinia (29, 58), culminating in an interval of maximum organic carbon burial, which causes the positive CIE. Increased oceanic anoxia occurs concurrently with the onset of the main extinction event at the Pliensbachian/Toarcian boundary (17, 60), and the greatest extent of anoxia and euxinia occurs during the large, negative CIE interval (ref. 58 and this study). White arrows represent enhanced intervals of volcanism within phase 2 of the Karoo–Ferrar eruptive scenario (49). Timescale is derived from ref. 48. Note that the vertical bars representing ammonite species diversity in NW Europe and western North America are binned by regional ammonite zones, resulting in a slight offset between adjacent columns.

minima in the ocean that is recorded by Tl isotopes. The $^{187}Os/^{188}Os_i$ values decline soon after the Pliensbachian/Toarcian boundary (46, 51), suggesting that the rate of continental weathering declined. Thus, the sustained deoxygenation and elevated organic carbon burial (Figs. 3 and 4), evidenced by the thallium and carbon isotope records, respectively, were mediated by processes internal to the oceans rather than the continued, elevated supply of nutrients from rivers. Such internal processes could be lower oxygen solubility, changes in ocean circulation under a warming climate, and/or the enhanced recycling of bioessential nutrients, such as phosphorus, under more reducing conditions.

The Tl isotope trends during the negative CIE (i.e., the traditional T-OAE interval) also suggest that global bottom water redox did not remain constant over the event. The shift from −3.5 to −2 and a return to −3.5, observed in both Canada and Germany, indicate another deoxygenation event and decrease in the global burial of Mn oxides (Fig. 3). This perturbation likely occurred over ∼30 ky to 50 ky assuming the timescale of refs. 47 and 52 (the T-OAE negative CIE has been assigned a duration of ∼300 ky to 500 ky, which, locally, is represented in ∼4.5 m in Alberta) and linear sedimentation rates in Canada (from 11.345 m to 11.84 m in the section) (46). The continued positive shift in the Tl isotope data during the recovery limb of the negative CIE of the T-OAE would require further marine deoxygenation and an additional ∼25% reduction in global Mn oxide burial (32). The dissolution of Mn oxides could be driven by permanent anoxia or, more realistically, transient deoxygenation that includes seasonal, centennial, and/or longer timescales depending on local hydrography, water chemistry, and sedimentation rates. Both the Pliensbachian/Toarcian boundary and the onset of the traditional T-OAE interval are associated with increased Mn/Ca values (53, 54), which could be due to the increased dissolved Mn reservoir associated with the dissolution of Mn oxides and reduction of Mn oxide precipitation.

The traditional T-OAE interval (i.e., as defined by the negative CIE) is associated with the main phase of Karoo–Ferrar LIP magmatism (47, 49, 55). This magmatic pulse would have caused global warming and enhanced continental weathering, as suggested by numerical modeling and geochemical and sedimentological records (46, 51, 56, 57). The net result would have been marine eutrophication and intensified and more widespread oxygen minima (e.g., refs. 5, 46, and 57). The second $\varepsilon^{205}Tl$ shift during the rising limb of the T-OAE CIE is roughly coincident with previously interpreted maximum extents of water column sulfidic anoxia (i.e., euxinia) during this event (29, 58). This second deoxygenation event corresponds to a further decline in marine diversity (end of phase 3 in ref. 17), that is, a continuation and ultimately the acme of the event that started at the Pliensbachian/Toarcian boundary (15, 16, 59–61) (Fig. 4). Given that these major losses in marine diversity occur coincidently with changes observed in the Tl isotope record (Fig. 4), ocean deoxygenation is implied as a significant or even the ultimate driver of extinction during this time. This interpretation does not, however, preclude a role by other environmental changes that may have occurred over this time in response to increasing pCO_2 (e.g., global warming and ocean acidification).

Interestingly, the $\varepsilon^{205}Tl$ data do not immediately return to preevent values after the peak of the positive CIE and remain high through the Falciferum and lower Bifrons zones $\delta^{13}C$ declines (Fig. 3). A similar pattern has been observed in the Tl isotope record of OAE-2 marked by values that remain high well after the end of the positive CIE (36). The decoupling of the two isotope systems suggests that global Mn oxide burial remained low and bottom water oxygen minima continued well after the termination of globally enhanced organic carbon burial rates during both OAEs.

One interpretation for this observation could be that, while overall organic carbon burial declined, productivity was sufficiently high to maintain the consumption of deeper water oxygen renewal (39). This scenario seems to be supported by the Os isotope record, which also remains elevated above preevent values over this same interval (46, 51) and indicates continued elevated continental weathering rates. Thus, the continued enhanced delivery of nutrients from weathering on the continents would have fueled elevated primary production that could have maintained the widespread expanded marine anoxia. Alternatively, large amounts of near-surface organic matter previously deposited during the event could have continued to drive bottom water oxygen consumption and Mn oxide dissolution during a time when new organic matter burial waned. This mechanism may also explain the elevated rates of pyrite burial inferred from the carbonate-associated sulfate sulfur isotope records that persist well after the CIE in both the T-OAE (58) and OAE-2 (62). Consumption of organic matter in shallowly buried sediments might have fueled marine anoxia and pyrite burial well after the CIEs, irrespective of the flux of newly exported organic matter.

Conclusions

The Tl isotope data presented here reveal more nuanced and explicit evidence for marine deoxygenation in the interval that surrounds the T-OAE, which began at the Pliensbachian/Toarcian boundary, and expanded oxygen minima were sustained throughout the early Toarcian and well after the traditionally defined T-OAE interval. Since the Tl isotope excursion begins at the Pliensbachian/Toarcian boundary, it generally corresponds with (*i*) the initiation of massive volcanism, (*ii*) a brief but significant increase in continental weathering, and (*iii*) the start of the protracted early Toarcian mass extinction event (17). Thus, this evidence for global marine deoxygenation provides a mechanism for the observed extinction record. Further, the current definition of the beginning of T-OAE, based on the start of the negative CIE and/or first occurrence of black shales in Europe, represents the nadir of the deterioration of environmental conditions, but not the onset of global deoxygenation.

The concept of an OAE was proposed due to the realization that the preservation of organic matter in marine sediments might not always be the product of local conditions. It followed that CIEs became the signature of enhanced burial of organic carbon on a global scale. Our study highlights the need to revisit our definition of the temporal OAE and consider whether the record of oceanic anoxia might be better defined by other geochemical proxies that reconstruct specific redox states of the global ocean. Perhaps more importantly, the acknowledgment that global deoxygenation may expand beyond the traditionally defined OAEs has important implications for our understanding of the environmental feedbacks that lead to and maintain these events. Identifying such processes would be key to determining the consequences and potential endpoints of the recent trend in deoxygenation in the oceans today.

ACKNOWLEDGMENTS. We thank Hannah Grove, Brett Holdaway, and Ashley Prow for laboratory assistance. We thank two anonymous reviewers whose comments greatly improved the manuscript. T.R.T. thanks the Florida State University Arts and Sciences Postdoctoral Fellowship, Geological Society of America, American Association of Petroleum Geologists, Society for Sedimentary Geology, and Virginia Polytechnic Institute and State University for funding. Grants to B.C.G. [National Science Foundation (NSF) EAR-1324752], J.D.O. and S.G.N. (NSF OCE-1624895 and NASA NNX16AJ60G), and T.W.L. (NSF EAR-0719911) also funded this work. A portion of this work was performed at the National High Magnetic Field Laboratory, which is supported by NSF Cooperative Agreement DMR-1157490 and the State of Florida. Alberta outcrop collections were authorized by the following permits: Parks Canada, Permit YHTR-2014-16156; Royal Tyrrell Museum of Palaeontology, Permits 13-058, 14-009, and 15-019.

1. Schmidtko S, Stramma L, Visbeck M (2017) Decline in global oceanic oxygen content during the past five decades. *Nature* 542:335–339.
2. Breitburg D, et al. (2018) Declining oxygen in the global ocean and coastal waters. *Science* 359:eaam7240.
3. Pálfy J, Smith PL (2000) Synchrony between Early Jurassic extinction, oceanic anoxic event, and the Karoo-Ferrar flood basalt volcanism. *Geology* 28:747–750.
4. Takashima R, Nishi H, Huber BT, Leckie RM (2006) Greenhouse world and the Mesozoic ocean. *Ocean* 19:64–74.

5. Jenkyns HC (2010) Geochemistry of oceanic anoxic events. *Geochem Geophys Geosyst* 11:Q03004.
6. Rothman DH (2017) Thresholds of catastrophe in the Earth system. *Sci Adv* 3: e1700906.
7. Keeling RE, Körtzinger A, Gruber N (2010) Ocean deoxygenation in a warming world. *Annu Rev Mar Sci* 2:199–229.
8. Long MC, et al. (2016) Finding forced trends in oceanic oxygen. *Global Biogeochem Cycles* 30:381–397.
9. Schlanger SO, Jenkyns HC (1976) Cretaceous oceanic anoxic events: Causes and consequences. *Geol Mijnb* 55:179–184.
10. Scholle PA, Arthur MA (1980) Carbon isotope fluctuations in cretaceous pelagic limestones: Potential stratigraphic and petroleum exploration tool. *Am Assoc Pet Geol Bull* 64:67–87.
11. Schlanger SO, Arthur MA, Jenkyns HC, Scholle PA (1987) The Cenomanian-Turonian Oceanic Anoxic Event, I. Stratigraphy and distribution of organic carbon-rich beds and the marine δ13C excursion. *Marine Petroleum Source Rocks*, Special Publications eds Brooks J, Fleet AJ (Geol Soc, London), Vol 26, pp 371–399.
12. Arthur MA, Dean WE, Pratt LM (1988) Geochemical and climatic effects of increased marine organic carbon burial at the Cenomanian/Turonian boundary. *Nature* 335: 714–717.
13. Jenkyns HC (1988) The early Toarcian (Jurassic) anoxic event: Stratigraphic, sedimentary, and geochemical evidence. *Am J Sci* 19:101–151.
14. Hesselbo SP, et al. (2000) Massive dissociation of gas hydrate during a Jurassic oceanic anoxic event. *Nature* 406:392–395.
15. Harries PJ, Little CTS (1999) The early Toarcian (Early Jurassic) and the Cenomanian-Turonian (Late Cretaceous) mass extinctions: Similarities and contrasts. *Palaeogeogr Palaeoclimatol Palaeoecol* 154:39–66.
16. Dera G, et al. (2010) High-resolution dynamics of Early Jurassic marine extinctions: The case of Pliensbachian-Toarcian ammonites (Cephalopoda). *J Geol Soc London* 167: 21–33.
17. Caruthers AH, Smith PL, Gröcke DR (2013) The Pliensbachian-Toarcian (Early Jurassic) extinction, a global multi-phased event. *Palaeogeogr Palaeoclimatol Palaeoecol* 386: 104–118.
18. Hermoso M, et al. (2009) Expression of the Early Toarcian negative carbon-isotope excursion in separated microfractions (Jurassic, Paris Basin). *Earth Planet Sci Lett* 277: 194–203.
19. Them TR, II, et al. (2017) High-resolution carbon isotope records of the Toarcian oceanic anoxic event (Early Jurassic) from North America and implications for the global drivers of the Toarcian carbon cycle. *Earth Planet Sci Lett* 459:118–126.
20. Kump LR, Arthur MA (1999) Interpreting carbon-isotope excursions: Carbonates and organic matter. *Chem Geol* 161:181–198.
21. Tyson RV (2005) The "productivity versus preservation" controversy: Causes, flaws, and resolution. *The Deposition or Organic-Carbon-Rich Sediments: Models, Mechanisms, and Consequences*, Special Publication (Soc Econ Paleontol Mineral, Tulsa, OK), Vol 82, pp 17–33.
22. Middelburg JJ, Vlug T, Jaco F, van der Nat WA (1993) Organic matter mineralization in marine sediments. *Global Planet Change* 8:47–58.
23. Burdige DJ (2007) Preservation of organic matter in marine sediments: Controls, mechanisms, and an imbalance in sediment organic carbon budgets? *Chem Rev* 107: 467–485.
24. Canfield DE (1994) Factors influencing organic carbon preservation in marine sediments. *Chem Geol* 114:315–329.
25. Hartnett HE, Keil RG, Hedges JI, Devol AH (1998) Influence of oxygen exposure time on organic carbon preservation in continental margin sediments. *Nature* 391: 572–574.
26. Schouten S, et al. (2000) Effects of an oceanic anoxic event on the stable carbon isotopic composition of early Toarcian carbon. *Am J Sci* 300:1–22.
27. Pearce CR, Cohen AS, Coe AL, Burton KW (2008) Molybdenum isotope evidence for global ocean anoxia coupled with perturbations to the carbon cycle during the Early Jurassic. *Geology* 36:231–234.
28. French KL, Sepúlveda J, Trabucho-Alexandre J, Gröcke DR, Summons RE (2014) Organic geochemistry of the early Toarcian oceanic anoxic event in Hawsker Bottoms, Yorkshire, England. *Earth Planet Sci Lett* 390:116–127.
29. Dickson AJ, et al. (2017) Molybdenum-isotope chemostratigraphy and paleoceanography of the Toarcian Oceanic Anoxic Event (Early Jurassic). *Paleoceanography* 32: 813–829.
30. Rehkämper M, et al. (2002) Thallium isotope variations in seawater and hydrogenetic, diagenetic, and hydrothermal ferromanganese deposits. *Earth Plant Sci Lett* 197: 65–81.
31. Nielsen SG, Rehkämper M, Norman MD, Halliday AN, Harrison D (2006) Thallium isotopic evidence for ferromanganese sediments in the mantle source of Hawaiian basalts. *Nature* 439:314–317.
32. Owens JD, Nielsen SG, Horner TJ, Ostrander CM, Peterson LC (2017) Thallium-isotopic compositions of euxinic sediments as a proxy for global manganese-oxide burial. *Geochim Cosmochim Acta* 213:291–307.
33. Nielsen SG, Rehkämper M, Prytulak J (2017) Investigation and application of thallium isotope fractionation. *Rev Mineral Geochem* 82:759–798.
34. Nielsen SG, et al. (2011) Thallium isotopes in early diagenetic pyrite–A paleoredox proxy? *Geochim Cosmochim Acta* 75:6690–6704.
35. Nielsen SG, et al. (2013) Towards an understanding of thallium isotope fractionation during adsorption to manganese oxides. *Geochim Cosmochim Acta* 117:252–265.
36. Peacock CL, Moon EM (2012) Oxidative scavenging of thallium by birnessite: Explanation for thallium enrichment and stable isotope fractionation in marine ferromanganese precipitates. *Geochim Cosmochim Acta* 84:297–313.
37. Rehkämper M, Frank M, Halliday A (2004) Cenozoic marine geochemistry of thallium deduced from isotopic studies of ferromanganese crusts and pelagic sediments. *Earth Planet Sci Lett* 219:77–91.
38. Nielsen SG, et al. (2006) Hydrothermal fluid fluxes calculated from the isotopic mass balance of thallium in the ocean crust. *Earth Planet Sci Lett* 251:120–133.
39. Ostrander CM, Owens JD, Nielsen SG (2017) Constraining the rate of oceanic deoxygenation leading up to a Cretaceous Oceanic Anoxic Event (OAE-2: ∼94 Ma). *Sci Adv* 3:e1701020.
40. Nielsen SG, et al. (2009) Thallium isotope evidence for a permanent increase in marine organic carbon export in the early Eocene. *Earth Planet Sci Lett* 278:297–307.
41. Rue EL, Smith GJ, Cutter GA, Bruland KW (1997) The response of trace element redox couples to suboxic conditions in the water column. *Deep Sea Res Part I Oceanogr Res Pap* 44:113–134.
42. McArthur JM, Algeo TJ, van de Schootbrugge B, Li Q, Howarth RJ (2008) Basinal restriction, black shales, Re-Os dating, and the early Toarcian (Jurassic) oceanic anoxic event. *Paleoceanography* 23:PA4217.
43. Bura-Nakić E, et al. (2018) Coupled U-Mo abundances and isotopes in a small marine euxinic basin: Constraints on processes in euxinic basins. *Geochim Cosmochim Acta* 222:212–229.
44. Owens JD, Reinhard CT, Rohrssen M, Love GD, Lyons TW (2016) Empirical links between trace metal cycling and marine microbial ecology during a large perturbation to Earth's carbon cycle. *Earth Planet Sci Lett* 449:407–417.
45. Röhl H-J, Schmid-Röhl A, Oschmann W, Frimmel A, Schwark L (2001) The Posidonia Shale (Lower Toarcian) of SW-Germany: An oxygen-depleted ecosystem controlled by sea level and palaeoclimate. *Palaeogeogr Palaeoclimatol Palaeoecol* 169:273–299.
46. Them TR, et al. (2017) Evidence for rapid weathering response to climatic warming during the Toarcian Oceanic Anoxic Event. *Sci Rep* 7:5003.
47. Sell B, et al. (2014) Evaluating the temporal link between Karoo LIP and climatic-biologic events of the Toarcian stage with high-precision U-Pb geochronology. *Earth Planet Sci Lett* 408:48–56.
48. Ruhl M, et al. (2016) Astronomical constraints on the duration of the Early Jurassic Pliensbachian Stage and global climatic fluctuations. *Earth Planet Sci Lett* 455: 149–165.
49. Moulin M, et al. (2017) Eruptive history of the Karoo lava flows and their impact on early Jurassic environmental change. *J Geophys Res Sol Earth* 122:738–772.
50. Xu W, et al. (2018) Magnetostratigraphy of the Toarcian Stage (Lower Jurassic) or the Llandbedr (Mochras Farm) Borehole, Wales: basis for a global standard and implications for volcanic forcing of palaeoenvironmental change. *J Geol Soc* jgs2017-120.
51. Percival LME, et al. (2016) Osmium isotope evidence for two pulses of increased continental weathering linked to Early Jurassic volcanism and climate change. *Geology* 44:759–762.
52. Boulila S, et al. (2014) Astronomical calibration of the Toarcian stage: Implications for sequence stratigraphy and duration of the early Toarcian OAE. *Earth Planet Sci Lett* 386:98–111.
53. Hermoso M, et al. (2009) Global and local forcing of Early Toarcian seawater chemistry: A comparative study of different paleoceanographic settings (Paris and Lusitanian basins). *Paleoceanography* 24:PA4208.
54. Lu Z, Jenkyns HC, Rickaby REM (2010) Iodine to calcium ratios in marine carbonate as a paleo-redox proxy during oceanic anoxic events. *Geol* 38:1107–1110.
55. Burgess SD, Bowring SA, Fleming TH, Elliot DH (2015) High-precision geochronology links the Ferrar large igneous province with early-Jurassic ocean anoxia and biotic crisis. *Earth Planet Sci Lett* 415:90–99.
56. Dera G, Donnadieu Y (2012) Modeling evidence for global warming, Arctic seawater freshening, and sluggish oceanic circulation during the Early Toarcian anoxic event. *Paleoceanography* 27:PA2211.
57. Izumi K, Kemp DB, Itamiya S, Inui M (2018) Sedimentary evidence for enhanced hydrological cycling in response to rapid carbon release during the early Toarcian oceanic anoxic event. *Earth Planet Sci Lett* 481:162–170.
58. Gill BC, Lyons TW, Jenkyns HC (2011) A global perturbation to the sulfur cycle during the Toarcian oceanic anoxic event. *Earth Planet Sci Lett* 312:484–496.
59. Little CTS, Benton MJ (1995) Early Jurassic mass extinction: A global long-term event. *Geology* 23:495–498.
60. Aberhan M, Baumiller TK (2003) Selective extinction among Early Jurassic bivalves: A consequence of anoxia. *Geology* 31:1077–1080.
61. Caswell BA, Coe AL, Cohen AS (2009) New range data for marine invertebrate species across the early Toarcian (Early Jurassic) mass extinction. *J Geol Soc London* 166: 859–872.
62. Owens JD, et al. (2013) Sulfur isotopes track the global extent and dynamics of euxinia during Cretaceous Oceanic Anoxic Event 2. *Proc Natl Acad Sci USA* 110: 18407–18412.
63. Scotese CR (2001) *Atlas of Earth History* (PALEOMAP Project, Arlington, TX).
64. Dera G, et al. (2009) Water mass exchange and variations in seawater temperature in the NW Tethys during the early Jurassic: Evidence from neodymium and oxygen isotopes of fish teeth and belemnites. *Earth Planet Sci Lett* 286:198–207.